



# Radiative association of $P^+(^3P)$ and $O(^3P)$ for the $PO^+$ formation

Zhi Qin <sup>1,2</sup>, Peigen Hu,<sup>1,2</sup> Jing Li<sup>3★</sup> and Linhua Liu <sup>1,2,4★</sup>

<sup>1</sup>Optics and Thermal Radiation Research Center, Institute of Frontier and Interdisciplinary Science, Shandong University, Qingdao, Shandong 266237, China

<sup>2</sup>School of Energy and Power Engineering, Shandong University, Jinan, Shandong 250061, China

<sup>3</sup>School of Physics and Physical Engineering, Qufu Normal University, Qufu 273165, China

<sup>4</sup>School of Energy Science and Engineering, Harbin Institute of Technology, Harbin, Heilongjiang 150001, China

Accepted 2023 May 20. Received 2023 May 10; in original form 2023 March 9

## ABSTRACT

Phosphorus (P) is essential for the development of life since it is a fundamental element in many important biological molecules. Due to its biogenic importance, many astrochemists have begun to investigate the possibility of the phosphorus-bearing species formed in interstellar environments. Radiative association (RA) is a possible way for the formation of the phosphorus monoxide ion ( $PO^+$ ) in interstellar and related environments. Laboratory measurements are almost impossible to carry out, so theoretical calculations are essential for investigating such formation mechanism of  $PO^+$ . The quantum mechanical method is used to obtain its cross sections and rate coefficients. Thirty contributing processes for the computation of the total rate coefficient are considered, including 22 transition dipole processes and eight permanent dipole processes. The total rate coefficient varies little over the entire temperature range of 1–10 000 K and its magnitude is of the order of  $(4–8) \times 10^{-17} \text{ cm}^3 \text{ s}^{-1}$ . The  $2^1\Sigma^+ \rightarrow X^1\Sigma^+$  transition process dominates the formation of  $PO^+$  by RA over the entire temperature range considered here. The  $C^1\Pi \rightarrow X^1\Sigma^+$  and  $2^3\Sigma^+ \rightarrow a^3\Sigma^+$  are also relatively important, but their rate coefficients are about an order of magnitude smaller than that of the  $2^1\Sigma^+ \rightarrow X^1\Sigma^+$  channel. The obtained cross sections and rate coefficient can be used to model the P astrochemistry in the interstellar medium.

**Key words:** astrochemistry – molecular data – molecular processes – ISM: molecules.

## 1 INTRODUCTION

In the past few years, phosphorus-bearing (hereafter called P-bearing) species has attracted much attention from the astrobiological/astrochemical community since P is a fundamental component of many key biomolecules, such as deoxyribonucleic acid, ribonucleic acid, adenosine triphosphate, and phospholipids. Detection of P-bearing species may help in studying prebiotic chemicals, which might be delivered to early Earth from extraterrestrial space (Chyba et al. 1990). To date, several P-bearing molecules have been found in extraterrestrial space. PN and PO have been identified in the interstellar medium (ISM; Turner & Bally 1987; Ziurys 1987; Lefloch et al. 2016; Rivilla et al. 2016, 2018; Bergner et al. 2019; Fontani et al. 2019; Chantzios et al. 2020; Rivilla et al. 2020; Bernal, Koelemay & Ziurys 2021; Haasler et al. 2022).  $PH_3$  has been detected towards IRC+10216 and in the atmosphere of Saturn (Bregman, Lester & Rank 1975; Agúndez et al. 2014), as well as in Venus' cloud decks (Villanueva et al. 2021; Greaves et al. 2021a, b; Bains et al. 2022). Moreover, CP, CCP, and HCP have been detected in the envelop of evolved stars (Agúndez, Cernicharo & Guélin 2007; Halfen, Clouthier & Ziurys 2008; Milam et al. 2008). Recently, the phosphorus monoxide ion ( $PO^+$ ) has been detected for the first time in the ISM (Rivilla et al. 2022).

$PO^+$  is the first P-bearing ion that detected in the ISM. The determined column density of  $PO^+$  by Rivilla et al. (2022) shows

that P is more efficiently ionized than N and S in the ISM. The ion  $P^+$  has been detected in several diffuse clouds (Jura & York 1978) with a cosmic abundance of  $\sim 2 \times 10^{-17}$  in hot regions ( $\sim 1200$  K) while the depletion of P was low (Jura & York 1978; Lebouteiller et al. 2006). Rivilla et al. (2022) also analysed the molecular abundance of  $PO^+$ , which is relatively high with respect to other P-containing species and indicates that  $PO^+$  plays an important role in the interstellar chemistry of P. Rivilla et al. (2022) analysed the formation mechanisms of  $PO^+$ , including the collision reaction of  $P^+ + OH \rightarrow PO^+ + H$  and the cosmic ray (CR) ionization reaction of  $PO + CR\text{-photon} \rightarrow PO^+ + e^-$ . Although several efforts have been devoted to understanding the chemistry of P in the ISM (Thorne et al. 1984; Fontani et al. 2016; Rivilla et al. 2018; Chantzios et al. 2020; Sil et al. 2021; Baptista & de Almeida 2023), many possible chemical pathways are still poorly characterized and unexplored.

To attain a better understanding of the P chemistry in the ISM, we concentrate on a possible pathway of the  $PO^+$  formation by radiative association (RA), that is,



As shown in equation (1), in the RA of the ionic  $P^+$  and the atomic O, these two species approach along the potential energy curve (PEC) of the diatomic  $PO^+$ . At any point of the PEC, spontaneous transitions into the bound levels of a lower electronic state may occur and a stable  $PO^+$  is formed by the emission of a photon. RA processes are difficult to measure in the laboratory (Gerlich & Horning 1992; Gustafsson

\* E-mail: jli@qfnu.edu.cn (JL); liulinhua@sdu.edu.cn (LL)

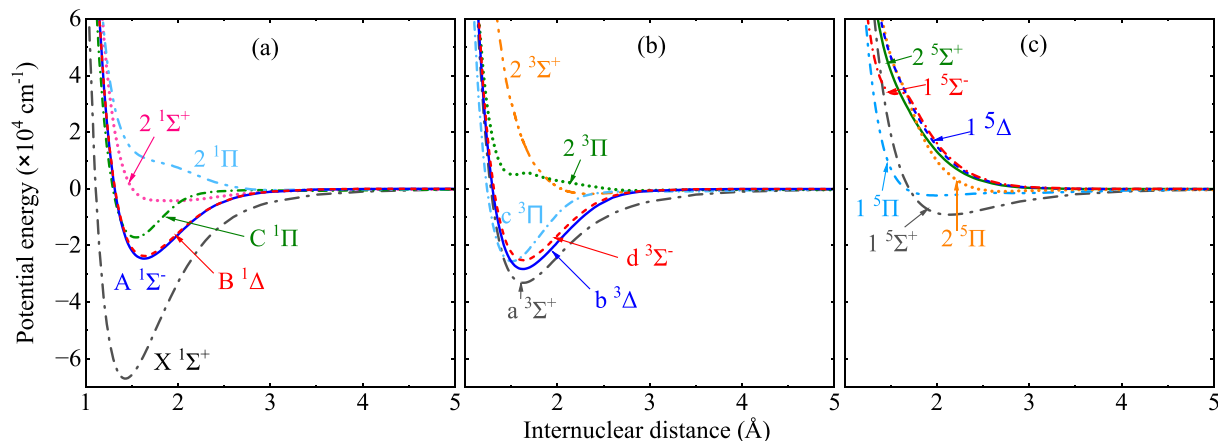


**Figure 1.** Potential energy curves of the (a) singlet, (b) triplet, and (c) quintet electronic states for  $PO^+$  calculated at the icMRCI/aug-cc-pwCV5Z-DK level of theory.

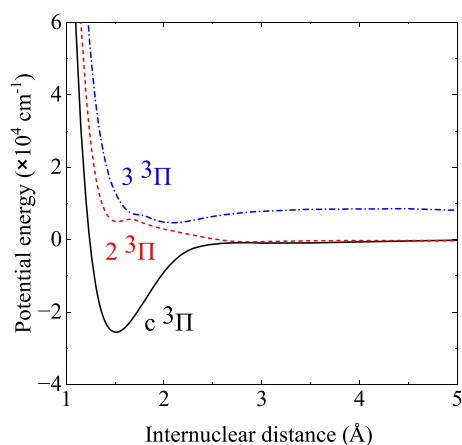


**Figure 2.** Potential energy curves of the first three  $^3\Pi$  states.

2020); hence, calculations of RA are of great importance. In the last 20 years, RA cross sections and rate coefficients for many diatomic molecules have been calculated with the semiclassical and high-level quantum mechanical methods (Barinovs & van Hemert 2006; Antipov et al. 2009; Franz, Gustafsson & Nyman 2011; Andrezza et al. 2012, 2020; Andrezza & de Almeida 2014; Gustafsson, Monge-Palacios & Nyman 2014; Nyman, Gustafsson & Antipov 2015; Andrezza, de Almeida & Borin 2016; Babb & McLaughlin 2017; Kathir, Nyman & Gustafsson 2017; Szabó & Gustafsson 2017, 2019; Andrezza, de Almeida & Vichiatti 2018; Forrey et al. 2018; Gustafsson & Forrey 2019; Zámečníková et al. 2019, 2020; Babb, Smyth & McLaughlin 2019a, b; Gustafsson 2020; Bai, Qin & Liu 2021, 2022; Qin, Bai & Liu 2021; Szabó, Góger & Gustafsson 2021; Meng, Qin & Liu 2022; Šimsová-Zámečníková, Soldán & Gustafsson 2022; Zhang, Qin & Liu 2022; Hou, Qin & Liu 2023), including two P-bearing molecules (namely PO and PS). RA for the formation of some molecules, such as SiO,  $O_2$ , and so on, had been used for astrochemistry modelling in the ejecta of Population III supernovae (SNe; Cherchneff & Dwek 2009) and in the Type Ibc SNe (Liljegren et al. 2022). The formation of the  $PO^+$  molecule through RA has not been investigated yet. As a reaction process of

RA for forming  $PO^+$ , it will contribute to understanding P chemistry in the ISM.

The aim of this work is to investigate the  $PO^+$  formation by RA. *Ab initio* PECs, transition dipole moments (TDMs), and permanent dipole moments (PDMs) are obtained using the state-of-the-art quantum chemistry methods. RA cross sections and rate coefficients are computed using the quantum mechanical perturbation theory (PT). These theory and methods are presented in Section 2. Section 3 presents our results and discussions. In Section 4, conclusion is drawn.

## 2 THEORY AND METHODS

### 2.1 Potential energy and (transition) dipole moment curves

To investigate the RA of  $P^+(3s^23p^2\ ^3P)$  and  $O(2s^22p^4\ ^3P)$ , the first thing is to obtain the PECs, TDMs, and PDMs of  $PO^+$  correlating to its first dissociation limit  $P^+(3s^23p^2\ ^3P) + O(2s^22p^4\ ^3P)$ . Based on Wigner–Witmer rules (Herzberg 1950), the first dissociation limit corresponds to 18 electronic states, including  $X^1\Sigma^+$ ,  $A^1\Sigma^-$ ,  $B^1\Delta$ ,  $C^1\Pi$ ,  $2^1\Sigma^+$ ,  $2^1\Pi$ ,  $a^3\Sigma^+$ ,  $b^3\Delta$ ,  $c^3\Pi$ ,  $d^3\Sigma^-$ ,  $2^3\Sigma^+$ ,  $2^3\Pi$ ,  $1^5\Sigma^+$ ,  $1^5\Delta$ ,  $1^5\Pi$ ,  $1^5\Sigma^-$ ,  $2^5\Sigma^+$ , and  $2^5\Pi$ . The PECs, TDMs, and PDMs for these electronic states were computed using MOLPRO 2015 quantum chemistry package (Werner et al. 2015, 2020). Initial molecular orbital (MO) and energy of the ground state were calculated by the Hartree–Fock method. Then, the state-averaged complete active space self-consistent field (SA-CASSCF) method was used for these 18 electronic states, yielding optimized MOs, and multiconfiguration wavefunctions (Knowles & Werner 1985; Werner & Knowles 1985). Finally, the dynamic electron correlation was treated using the internally contracted multireference configuration interaction (icMRCI) method based on a subset of the SA-CASSCF optimized multiconfiguration wavefunctions, and the Davidson correction (+Q) was also included to consider the size-consistency error (Langhoff & Davidson 1974). PECs, TDMs, and PDMs for singlet and triplet states were generated for a total of 68 single points spanning internuclear distances from 1.0 to 7.5  $\text{\AA}$ . PECs, TDMs, and PDMs for quintet states were generated for a total of 65 single points spanning internuclear distances from 1.2 to 7.5  $\text{\AA}$ . Near the equilibrium region, the points were refined and spaced by 0.02  $\text{\AA}$ .

**Table 1.** Spectroscopic constants for the electronic states by the present icMRCI + Q/aug-cc-pwCV5Z-DK calculation, along with other theoretical and experimental results.

State	Source	$R_e$ (Å)	$T_e$ (Å)	$\omega_e$ (cm <sup>-1</sup> )	$\omega_e\chi_e$ (cm <sup>-1</sup> )	$\omega_e y_e$ (cm <sup>-1</sup> )	$B_e$ (cm <sup>-1</sup> )	$10^2\alpha_e$ (cm <sup>-1</sup> )	$D_e$ (cm <sup>-1</sup> )
$X^1\Sigma^+$	This work	1.4300	0.00	1406.18	7.26	0.013 41	0.781 73	0.544	66 743.19
	Exp. <sup>a</sup>	1.4250	0.00	1411.53	7.11		0.7870		
	Exp. <sup>b</sup>	1.419 ± 0.005	0.00	1410 ± 30	10 ± 20				66 540.71 ± 80.66
	Exp. <sup>c</sup>			1405					
	Cal. <sup>d</sup>	1.4225	0.00	1411.12	5.732	0.0370	0.789 89	0.551	
	Cal. <sup>e</sup>	1.4262	0.00	1411.96	7.5336	0.128 83	0.7856	0.5536	67 545.68
	Cal. <sup>f</sup>	1.4301	0.00	1411.3	7.88		0.781 39	0.554	
$a^3\Sigma^+$	This work	1.6268	33 856.66	899.56	3.31	-0.133 11	0.602 66	0.495	33 591.27
	Cal. <sup>d</sup>	1.6103	34 375.04	938.28	8.770	0.0295	0.616 44	0.612	
	Cal. <sup>e</sup>	1.6180	34 359.63	938.96	7.474	0.3745	0.6106	0.535	33 205.83
$b^3\Delta$	This work	1.6272	38 663.86	913.98	5.46	0.003 65	0.603 58	0.505	28 879.80
	Cal. <sup>d</sup>	1.6091	39 395.00	956.28	6.746	0.1350	0.617 27	0.543	
	Cal. <sup>e</sup>	1.6163	39 280.91	949.21	6.812	0.8444	0.6120	0.495	28 326.18
$c^3\Pi$	This work	1.5088	41 467.80	1091.44	7.20	-0.029 92	0.701 97	0.609	25 949.71
	Cal. <sup>d</sup>	1.5005	42 015.69	1107.00	6.843	0.2953	0.709 75	0.503	
	Cal. <sup>e</sup>	1.5047	41 996.03	1108.65	7.745	0.2037	0.7058	0.581	25 549.21
$d^3\Sigma^-$	This work	1.6336	41 846.59	891.84	5.50	-0.005 43	0.598 86	0.516	25 951.25
	Cal. <sup>d</sup>	1.6125	42 493.05	925.31	6.912	0.1790	0.614 69	0.563	
	Cal. <sup>e</sup>	1.6208	42 445.95	924.02	9.192	0.1207	0.6085	0.611	25 162.07
$A^1\Sigma^-$	This work	1.6340	42 319.91	887.11	5.87	-0.005 42	0.598 83	0.545	25 362.95
	Cal. <sup>d</sup>	1.6127	43 085.40	939.98	8.034	0.0089	0.614 25	0.597	
	Cal. <sup>e</sup>	1.6208	43 058.95	920.57	9.280	0.0080	0.6085	0.628	24 539.41
$B^1\Delta$	This work	1.6351	43 238.30	873.39	6.08	-0.008 76	0.598 03	0.569	23 744.25
	Cal. <sup>d</sup>	1.6119	44 125.34	912.19	9.200	0.0420	0.615 19	0.648	
	Cal. <sup>e</sup>	1.6200	44 101.23	907.82	8.739	0.0392	0.6089	0.627	23 526.37
$C^1\Pi$	This work	1.5430	49 812.09	1007.56	7.50	-0.131 58	0.670 89	0.602	16 692.37
	Exp. <sup>c</sup>		49 930	1017					
	Cal. <sup>d</sup>	1.5315	49 996.15	1017.39	1.139	0.6006	0.636 49	1.919	
$1^5\Sigma^+$	This work	1.5348	50 005.98	1015.91	1.030	0.3511	0.6802	0.594	17 527.23
	This work	2.1351	57 911.41	388.10	3.75	-0.013 57	0.350 55	0.425	9147.95
	Cal. <sup>e</sup>	2.1225	58 741.07	402.02	4.3725	0.183 23	0.3550	0.420	8831.77
$2^1\Sigma^+$	This work	1.9396	62 771.54	168.14	-11.80	-0.6619	0.451 43	0.939	4095.84
	Cal. <sup>e</sup>	2.0192	63 859.44	258.67	0.2811	0.404 43	0.3900	0.6074	3738.38
$1^5\Pi$	This work	1.9948	64 709.75	232.85	7.39	-0.1189	0.400 22	1.36	2299.64
	Cal. <sup>e</sup>	2.0018	65 320.04	237.28	18.985	3.0215	0.3945	1.9090	2229.32

<sup>a</sup> Petrmichl et al. (1991).<sup>b</sup> Dyke et al. (1982).<sup>c</sup> Dressler (1955).<sup>d</sup> Zhang & Shi (2021).<sup>e</sup> Zhu et al. (2014).<sup>f</sup> Metropoulos et al. (2003).

The full point group of  $\text{PO}^+$  is  $C_{\infty v}$ , which cannot be used directly in MOLPRO. Calculations were carried out at  $C_{2v}$  symmetry, which is the largest Abelian subgroup of  $C_{\infty v}$ . The mapping relationships between the irreducible representations of  $C_{\infty v}$  and those of  $C_{2v}$  are as follows:

$$\begin{aligned} \Sigma^+ &\rightarrow A_1 & \Sigma^- &\rightarrow A_2 \\ \Pi &\rightarrow (B_1, B_2) & \Delta &\rightarrow (A_1, A_2) \end{aligned} \quad (2)$$

During the calculations, the augmented correlation consistent polarized weighted core–valence basis set aug-cc-pwCV5Z-DK was chosen for  $\text{P}^+$  and  $\text{O}$ . Electrons in inner shells (namely  $1s2s2p$  shells of  $\text{P}^+$  and  $1s$  shell of  $\text{O}$ ) were kept closed and double-occupied in the reference space. The remaining 10 electrons were put into the active space. The scalar relativistic effect was taken into account by the third-order Douglas–Kroll–Hamiltonian approximation (Reiher & Wolf 2004a, b).

**Table 2.** Fitting parameters for the three-parameter Arrhenius–Kooij function obtained by fitting the RA rate coefficient in the formation of PO<sup>+</sup>.

$T$ (K)	$A$ (cm <sup>3</sup> s <sup>-1</sup> /10 <sup>-17</sup> )	$\alpha$	$\beta$
1–10	9.342 54	0.149 93	-0.165 24
10–30	6.365 47	-0.002 67	1.188 99
30–120	7.018 71	0.060 45	-0.257 74
120–300	7.027 08	0.023 15	4.032 88
300–800	7.391 34	-0.021 36	19.487 05
800–1300	8.328 31	-0.083 11	66.819 73
1300–2000	7.531 20	-0.042 86	12.627 75
2000–5000	4.274 57	0.145 322	-410.724 03
5000–	3.778 39	0.183 60	-491.971 791
10 000			

## 2.2 Radiative association cross sections and rate coefficients

The cross section of RA for a transition  $f \leftarrow i$  can be obtained by the quantum mechanical PT, which yields the following expression

$$\sigma_{f \leftarrow i}(E_c) = \sum_{J_i; v_f, J_f} \frac{1}{4\pi\epsilon_0} \frac{64}{3} \frac{\pi^5}{k^2} p_i \times \frac{S_{J_f \leftarrow J_i}}{\lambda_{J_i; v_f, J_f}^3(E_c)} |M_{J_i; v_f, J_f}(E_c)|^2, \quad (3)$$

where the sum runs over the angular momentum of the initial electronic state ( $J_i$ ), and the vibrational ( $v_f$ ) and rotational ( $J_f$ ) quantum numbers of the final electronic state.  $\epsilon_0$  is the vacuum permittivity.  $k^2 = 2\mu E_c/\hbar^2$ ,  $\mu$  is the reduced mass of the colliding fragments,  $E_c$  is the collision energy, and  $\hbar$  is the reduced Planck constant.  $\lambda_{J_i; v_f, J_f}$  is the wavelength of the emitted photon, and  $S_{J_f \leftarrow J_i}$  is the Hönl–London factor (Hansson & Watson 2005; Watson 2008), depending on a specific electronic transition process. In this work, we chose the criterion used in previous papers (Zámečníková et al. 2020; Qin et al. 2021; Meng et al. 2022) to compute the Hönl–London factors.  $p_i$  is the statistical weight (or the probability of collision in the initial electronic state), determined by initial atomic and final molecular electronic states.  $M_{J_i; v_f, J_f}$  is the transition dipole matrix elements, defined by

$$M_{J_i; v_f, J_f}(E_c) = \int_0^\infty \chi_{J_i}(E_c; R) D(R) \psi_{v_f, J_f}(R) dR, \quad (4)$$

where  $D(R)$  is the TDM or PDM,  $\chi_{J_i}(E_c; R)$  is the radial wavefunction of an initial continuum state, and  $\psi_{v_f, J_f}$  is the radial part of the ro-vibrational wavefunction of a final bound state. The renormalized Numerov method (Johnson 1977, 1978) was used to obtain the bound and continuum wavefunctions.

The thermal rate coefficient for a  $f \leftarrow i$  transition can be computed from the cross section

$$k_{f \leftarrow i}(T) = \left(\frac{8}{\mu\pi}\right)^{1/2} \left(\frac{1}{k_B T}\right)^{3/2} \int_0^\infty E_c \sigma_{f \leftarrow i}(E_c) \times \exp\left(-\frac{E_c}{k_B T}\right) dE_c, \quad (5)$$

where  $k_B$  is the Boltzmann constant,  $k_B = 1.381 \times 10^{-23}$  J·K<sup>-1</sup>.

## 3 RESULTS AND DISCUSSION

### 3.1 Potential energy curves and transition dipole moments

The PECs of singlet, triplet, and quintet electronic states for PO<sup>+</sup> correlating to its first dissociation limit P<sup>+</sup>(3s<sup>2</sup>3p<sup>2</sup> <sup>3</sup>P) + O(2s<sup>2</sup>2p<sup>4</sup>

<sup>3</sup>P) were considered and presented in Fig. 1 versus the internuclear distance  $R$ . Comparing the PECs with those given by Zhu et al. (2014), they are similar in shape. The 2 <sup>3</sup>Π state exhibits an avoided crossing at  $R \approx 1.7$  Å due to a non-adiabatic coupling with the dissociative 3 <sup>3</sup>Π state, resulting in a dissociative character for the 2 <sup>3</sup>Π state in the long-range region, as shown in Fig. 2. Similarly, the 1 <sup>5</sup>Σ<sup>-</sup> state exhibits an avoid crossing at  $R \approx 1.68$  Å with the 2 <sup>5</sup>Σ<sup>-</sup> state. It is worth mentioning that the A <sup>1</sup>Σ<sup>-</sup> and B <sup>1</sup>Δ states lie very close along the whole internuclear distance considered in our calculations.

Table 1 compares the spectroscopic constants, including the electronic excitation energy relative to the ground state,  $T_e$  (cm<sup>-1</sup>), equilibrium internuclear distance,  $R_e$  (Å), harmonic frequency,  $\omega_e$  (cm<sup>-1</sup>), first-order anharmonic constant,  $\omega_e \chi_e$  (cm<sup>-1</sup>), rotation constant,  $B_e$  (cm<sup>-1</sup>), and ro-vibrational coupling constant,  $\alpha_e$  (cm<sup>-1</sup>), of 11 lowest electronic states of PO<sup>+</sup> to those from previous calculations (Metropoulos, Papakondylis & Mavridis 2003; Zhu et al. 2014; Zhang & Shi 2021) and experiments (Dyke, Morris & Ridha 1982; Petrmichl, Peterson & Woods 1991). Many theoretical studies have been carried out on the spectroscopic constants of the ground X <sup>1</sup>Σ<sup>+</sup> state for PO<sup>+</sup> (Peterson & Woods 1988, 1990; Wong & Radom 1990; Spielfiedel & Handy 1999; Martin & Fehér 2001; Metropoulos et al. 2003), and Table 1 presents the results from the recent three papers. Our spectroscopic constants show good agreement with both experimental and theoretical values, with better agreement with the experiment than previous calculations for the dissociation energy. For other electronic states, our electronic excitation energies and harmonic frequencies are slightly smaller than those computed by Zhu et al. (2014) and Zhang et al. (2021), which is mainly caused by the different theoretical levels used.

For the long-range region at  $R > 7.5$  Å, the PECs were fitted by the following function (Tomza et al. 2019):

$$V(R) = -\frac{C_3^{\text{elst}}}{R^3} - \frac{C_4^{\text{ind}}}{R^4}, \quad (6)$$

where  $C_3^{\text{elst}}/R^3$  describes the electrostatic interaction between the charge of the ion (P<sup>+</sup>) and the quadrupole moment of the atom (O),  $C_4^{\text{ind}}$  is caused by an induced atomic dipole of O due to the electric field of the ion (P<sup>+</sup>), which is related to the static dipole polarizability  $\alpha$  of the atomic O by

$$C_4^{\text{ind}} = \frac{Q^2 \alpha(O)}{2}, \quad (7)$$

where  $Q$  is the charge of the ion. In this work, we used the  $\alpha(O)$  value of 5.2 au measured by Salop et al. (1961). Wang et al. (2021) also presented  $\alpha(O) = 5.21$  using the explicitly correlated coupled cluster method.  $C_3^{\text{elst}}$  was obtained by fitting *ab initio* energy points while keeping  $C_4^{\text{ind}}$  fixed. Note that equation (7) assumes atomic units, so it should be converted into cm<sup>-1</sup> when fitting *ab initio* energy points. For  $R < 0.8$  Å, the PECs were extrapolated by the following function:

$$V(R) = A \exp(-BR) + C, \quad (8)$$

where  $A$ ,  $B$ , and  $C$  are fitting parameters.

Fig. 3 plots the TDMs of dipole-allowed transitions for singlet, triplet, and quintet states of PO<sup>+</sup>. The TDMs tend to be zero in the long-range limit. In a fixed frame of reference centred on the centre of mass, the PDMs for singlet, triplet, and quintet states of PO<sup>+</sup> are obtained and shown in Fig. 4. The PDMs approach non-zero in the long-range limit, approximately equal to  $(-0.655R + 0.11)$  at large internuclear distances ( $R > 5$  Å). This value is estimated using the calculated PDM values at  $R > 5$  Å. That is, the PDM value varies linearly at  $R > 5$  Å. For example, the PDM value is

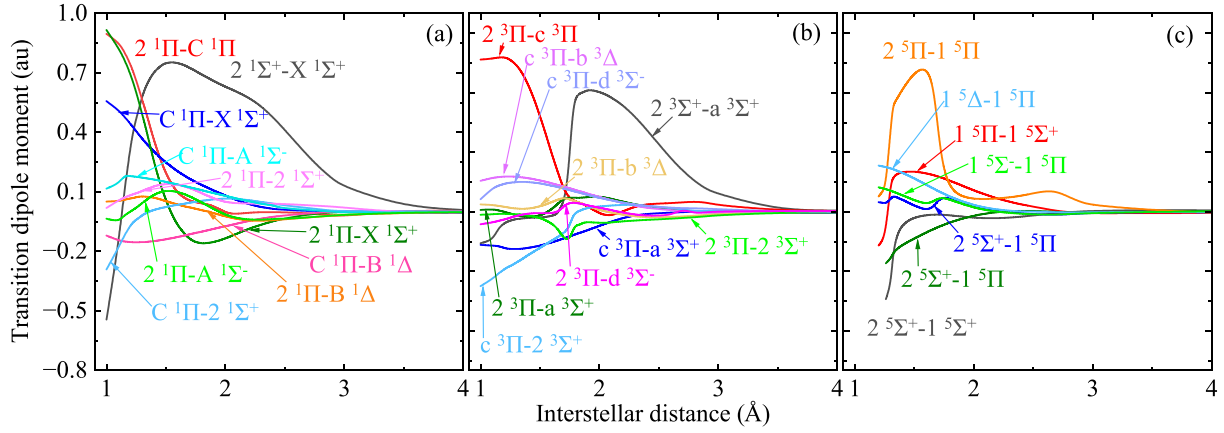


**Figure 3.** Transition dipole moments for the (a) singlet, (b) triplet, and (c) quintet transitions of  $\text{PO}^+$  as a function of the internuclear distance  $R$ .

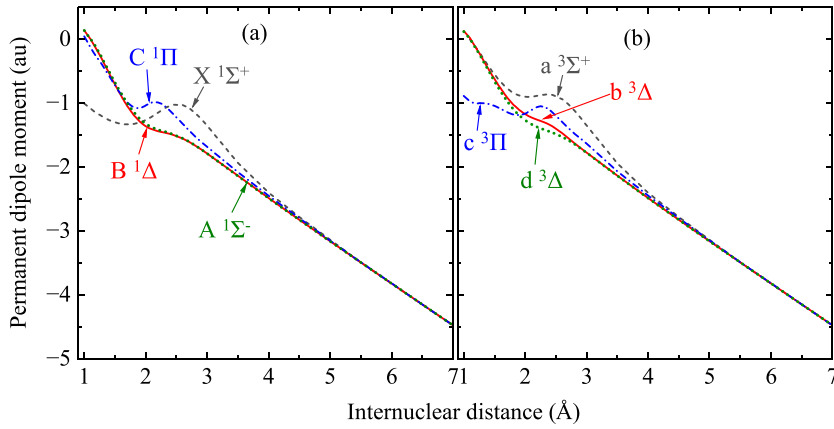


**Figure 4.** Permanent dipole moment for (a) the  $X^1\Sigma^+$ ,  $B^1\Delta$ ,  $C^1\Pi$ , and  $A^1\Sigma^-$  states, and (b) the  $a^3\Sigma^+$ ,  $b^3\Delta$ ,  $c^3\Pi$ , and  $d^3\Sigma^-$  states of  $\text{PO}^+$ .

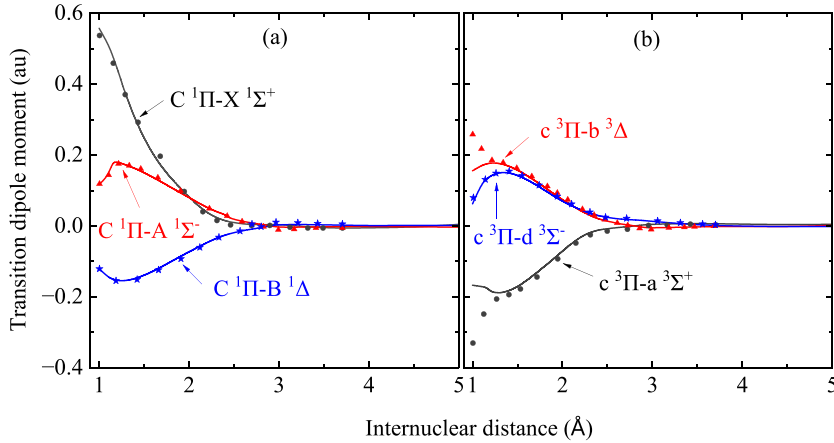


**Figure 5.** Comparison of the transition dipole moments of (a) the  $C^1\Pi - X^1\Sigma^+$ ,  $C^1\Pi - A^1\Sigma^-$ , and  $C^1\Pi - B^1\Delta$  system, and (b) the  $c^3\Pi - a^3\Sigma^+$ ,  $c^3\Pi - b^3\Delta$  and  $c^3\Pi - d^3\Sigma^-$  systems for  $\text{PO}^+$ . The lines are from this work; the symbols represent the computed values from Zhang & Shi (2021).

close to  $(-0.655 \times 5 + 0.11) = -3.165$  au when  $R = 5$  Å. Also, the PDM value is close to  $(-0.655 \times 7 + 0.11) = -4.475$  au when  $R = 7$  Å. Such situation is similar to the  $A^2\Pi_u - X^2\Pi_g$  TDM of  $\text{O}_2^+$  (Wetmore, Fox & Dalgarno 1984), also similar to the TDMs of the  $B^4\Sigma_u^- - X^4\Sigma_g^-$ ,  $f^2\Pi_g - a^2\Pi_u$ , and  $2^2\Pi_g - 2^2\Pi_u$  transitions for  $\text{C}_2^+$  (Babb, Smyth & McLaughlin 2019b). Comparison of the

TDMs for the  $C^1\Pi - X^1\Sigma^+$ ,  $C^1\Pi - A^1\Sigma^-$ ,  $C^1\Pi - B^1\Delta$ , and  $c^3\Pi - d^3\Sigma^-$  systems with those provided by Zhang & Shi (2021) shows overall good agreements up to the dissociation limits. However, there exist slight deviations for the PDMs at internuclear distances below 1.25 Å for the  $c^3\Pi - a^3\Sigma^+$  and  $c^3\Pi - b^3\Delta$  systems.

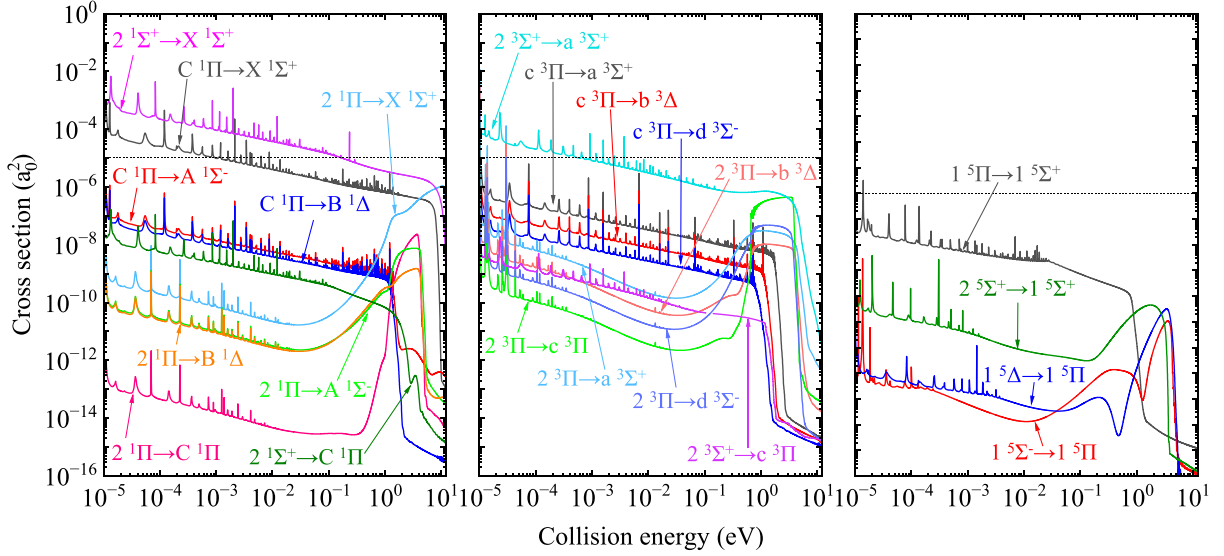


**Figure 6.** Radiative association cross sections (in units of  $a_0^2$ ) of dipole-allowed transitions for (a) singlet, (b) triplet, and (c) quintet states in the collision of  $P^+(3s^23p^2\ ^3P)$  and  $O(2s^22p^4\ ^3P)$ .

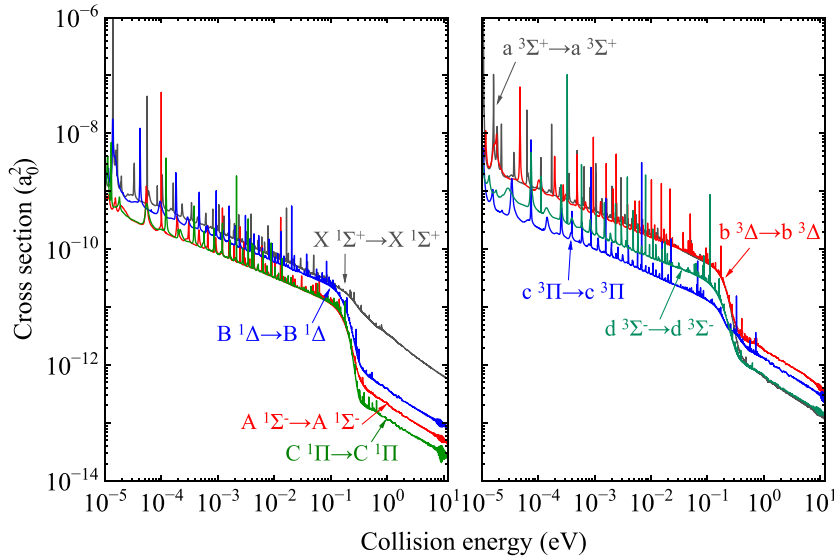


**Figure 7.** Radiative association cross sections (in units of  $a_0^2$ ) of permanent dipole transitions for (a) singlet and (b) triplet states in the collision of  $P^+(3s^23p^2\ ^3P)$  and  $O(2s^22p^4\ ^3P)$ .

### 3.2 Radiative association cross sections

For the total 18 electronic states correlating to the  $P^+(3s^23p^2\ ^3P) + O(2s^22p^4\ ^3P)$  dissociation limit of  $PO^+$ , we considered nine singlet, nine triplet, and four quintet transitions for different electronic states (as shown in Fig. 6), as well as eight permanent dipole transitions (as shown in Fig. 7). Other transitions are not considered here because the states involved these transitions either have shallow potential wells or are completely repulsive, which are expected to contribute little to the RA in the collision of  $P^+(3s^23p^2\ ^3P)$  and  $O(2s^22p^4\ ^3P)$ . Numerous shape resonances are visible in Figs 6 and 7. For transitions between PECs with deep potential wells, their RA cross sections are more dominant at lower collision energies and their contributions are still significant up to  $E_c = 1.0$  eV, such as for the  $C^1\Pi - A^1\Sigma^-$ ,  $C^1\Pi - B^1\Delta^-$ ,  $c^3\Pi - a^3\Sigma^-$  transitions, and so on, some

even to  $E_c = 6.0$  eV, such as for the  $2^1\Sigma^+ - X^1\Sigma^+$ ,  $2^1\Sigma^+ - C^1\Pi$ , and so on. Previous studies (Szabó et al. 2021; Kramida et al. 2022) indicate that the bremsstrahlung, ionization, and electronic excitation may dominate above  $E_c = 1.0$  eV. For some transitions such as those from the  $2^3\Pi$  state to a  $^3\Sigma^+$ ,  $b^3\Delta$ ,  $c^3\Pi$ , and  $d^3\Sigma^-$  states, the resonance tunnelling features are visible because of the potential barrier (local maximum) on the PEC of the  $2^3\Pi$  state. The local maximum on the PEC of the  $2^3\Pi$  state is about 0.66 eV at  $R = 1.68$  Å, and the cross section for the transition from this state increases sharply above 0.66 eV. Similar situation also exists for the transitions from the  $2^1\Pi$  state to the  $X^1\Sigma^+$ ,  $A^1\Sigma^-$ ,  $B^1\Delta$ , and  $C^1\Pi$  states.

As shown in Fig. 6, the  $2^1\Sigma^+ \rightarrow X^1\Sigma^+$  transition contributes most along the whole collision energy considered here. The large

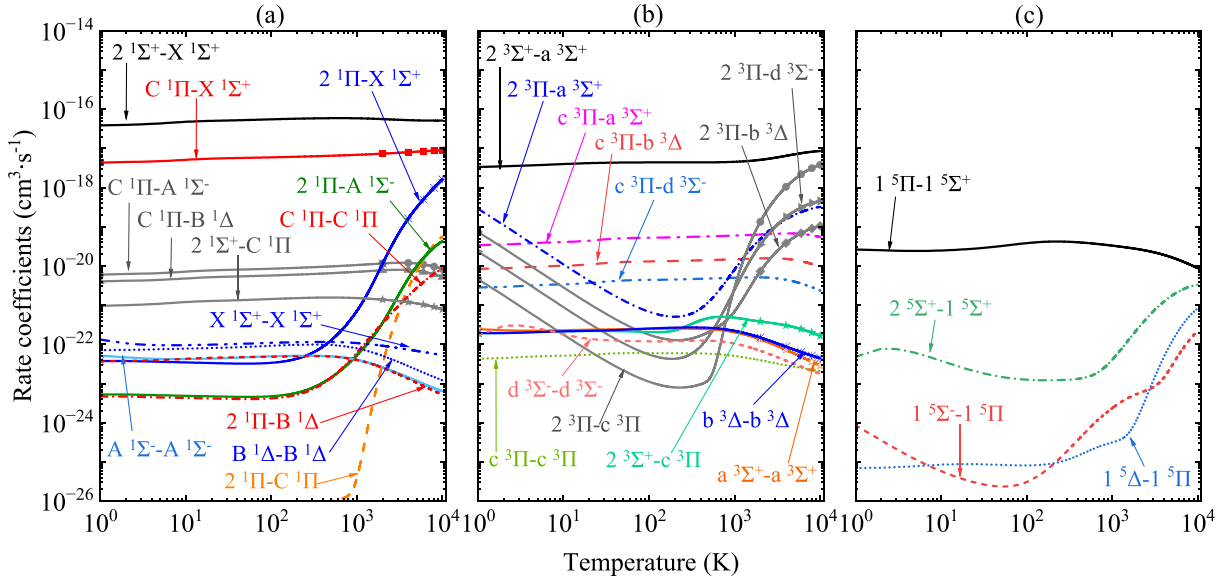


**Figure 8.** Rate coefficients (in units of  $\text{cm}^3 \text{s}^{-1}$ ) of (a) singlet transitions, (b) triplet transitions, and (c) quintet transitions for the formation of  $\text{PO}^+$  by the RA process (1).

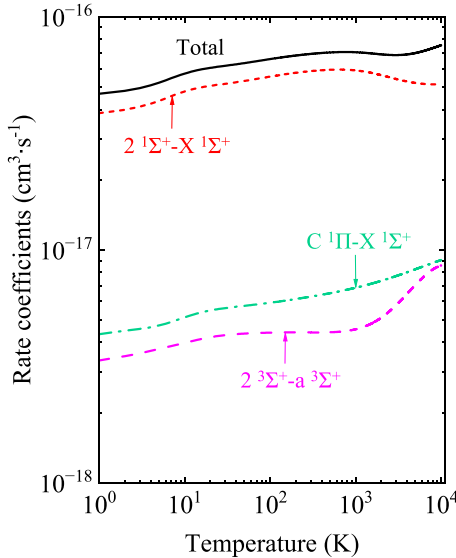


**Figure 9.** The total rate coefficient (in units of  $\text{cm}^3 \text{s}^{-1}$ ) for the formation of  $\text{PO}^+$  by RA. Rate coefficients for some important electronic transition processes are also presented.

cross section for the  $2^1\Sigma^+ \rightarrow X^1\Sigma^+$  transition is due to the large TDM, especially in the Franck–Condon region. Also, the  $X^1\Sigma^+$  state is very deep and can support many ro-vibrational bound levels to which RA transitions can occur. The  $C^1\Pi \rightarrow X^1\Sigma^+$  and  $2^3\Sigma^+ \rightarrow a^3\Sigma^+$  transitions are also relatively important and their RA cross sections are approximately an order of magnitude smaller than those of the  $2^1\Sigma^+ \rightarrow X^1\Sigma^+$  transition. The RA cross sections for other electronic transition processes are relatively unimportant except for the  $2^3\Pi \rightarrow c^3\Pi$  process at high-collision energies of about 0.7–3 eV. As given in Fig. 7, RA cross sections from permanent dipole transitions for all electronic states are small, nearly six orders of magnitude less than those of the  $2^1\Sigma^+ \rightarrow X^1\Sigma^+$  transition. They

are also theoretically expectedly low because of the one electronic-state nature.

### 3.3 Rate coefficients

Based on cross sections above, rate coefficients were calculated using equation (5). An overview of the rate coefficients is given in Fig. 8 for singlet, triplet, and quintet transitions. The total rate coefficient for the RA of  $\text{P}^+(3s^23p^2\ ^3P)$  and  $\text{O}(2s^22p^4\ ^3P)$  is presented in Fig. 9, along with those of several important electronic transitions. At the temperature range of 1 to 10000 K considered here, the total rate coefficient exhibits a slight variation, with the value of about  $(4\text{--}8) \times 10^{-17} \text{cm}^3 \text{s}^{-1}$ . The  $2^1\Sigma^+ \rightarrow X^1\Sigma^+$  transition plays a major role in this entire temperature range. The  $C^1\Pi \rightarrow X^1\Sigma^+$  and  $2^3\Sigma^+ \rightarrow a^3\Sigma^+$  transitions also provide a little contribution and their rate coefficients are approximately an order of magnitude smaller than that of the  $2^1\Sigma^+ \rightarrow X^1\Sigma^+$  transition. Other transitions contribute little to the total rate coefficient, as expected from the cross sections.

The obtained rate coefficient for the formation of  $\text{PO}^+$  by RA is used to fit the three-parameter Arrhenius–Kooij function (Laidler 1996):

$$k(T) = A \left( \frac{T}{300} \right)^\alpha e^{-\beta/T}, \quad (9)$$

where  $A$ ,  $\alpha$ , and  $\beta$  are fitting parameters. To well reproduce the rate coefficient, we divided the corresponding curve into several temperature ranges which were fitted individually. The fitting parameters are summarized in Table 2 for different temperature ranges.

The magnitude of the total rate coefficient is comparable to the formation of other diatomic molecules by RA (Nyman et al. 2015). As a reaction process for forming molecules, RA can be important in low-density regions with little dust or few grains of the interstellar space. The rate coefficients for the formation of many diatomic molecules, such as SiS,  $\text{SiO}^+$ , and SO, by RA were computed in previous studies. Some results had been included in the UMIST Database for Astrochemistry (UDfA; McElroy et al. 2013) and had been used for astrochemistry modelling in celestial bodies, such as

in the ejecta of Population III SNe (Cherchneff & Dwek 2009) and in the Type Ibc SNe (Liljegren et al. 2022).  $PO^+$  has been recently detected in astronomical environments (Rivilla et al. 2022). Here, we compute the rate coefficient for the formation of  $PO^+$  by RA, which is expected to be helpful for modelling the evolution of P in interstellar environments. Note that the RA rate coefficient is much smaller than those of chemical exchange reactions. Therefore, the RA process is likely to be ignored in high-density regions of astronomical environments, where various collisional reactions are dominant due to high density of chemical species.

Recently, Rivilla et al. (2022) detected two rotational transitions ( $J = 1-0$  and  $J = 2-1$ ) of  $PO^+$  in the ISM toward the molecular cloud G+0.693–0.027. The shocks sputter the interstellar icy grain mantles, releasing into most gas-phase P content, including most  $PH_3$ , which is converted into atomic P, and then ionized by CRs, forming  $P^+$ . Further reactions with  $O_2$  and OH produces  $PO^+$ . According to Rivilla et al. (2022), RA of  $P^+$  and O seems not to be noticed in the formation of  $PO^+$ . We expect that our RA rate coefficients for  $PO^+$  are helpful for modelling the P chemistry in the ISM with low dust. Rivilla et al. (2022) pointed out three phases in chemical modelling of  $PO^+$  toward the molecular cloud G+0.693–0.027 and the rate coefficients at temperatures of 10–20 K might be relevant if RA of  $P^+$  and O is considered.

## 4 CONCLUSIONS

In this work, we have calculated the total rate coefficient for the formation of  $PO^+$  through radiative associative of  $P^+$  and O in their electronic ground states, in which the temperatures of 1–10 000 K are considered. The quantum mechanical method is used to investigate a total of 30 RA processes. The cross section for each RA processes is obtained versus the collision energy from 0.000 01 to 10 eV. Analysis of the cross section shows that the RA process from  $2^1\Sigma^+ \rightarrow X^1\Sigma^+$  dominates the entire range of collision energy considered in this work. RA transition channels including  $C^1\Pi \rightarrow X^1\Sigma^+$  and  $2^3\Sigma^+ \rightarrow a^3\Sigma^+$  are also relatively important for the formation of  $PO^+$  and their cross sections are about an order of magnitude smaller than that of the  $2^1\Sigma^+ \rightarrow X^1\Sigma^+$  channel. Other RA channels, including quintet transitions and permanent dipole transitions, are almost no contribution to the formation of  $PO^+$ . The total rate coefficients for the formation of  $PO^+$  by RA are of the order of  $(4-8) \times 10^{-17} \text{ cm}^3 \text{ s}^{-1}$  for temperatures from 1 to 10 000 K. The obtained data can be utilized in the modelling of the  $PO^+$  abundance in the ISM.

## SUPPORTING INFORMATION

Supplementary data are available at [MNRAS](https://www.mnras.org/) online.

### Rate coefficient.txt

Please note: Oxford University Press is not responsible for the content or functionality of any supporting materials supplied by the authors. Any queries (other than missing material) should be directed to the corresponding author for the article.

## ACKNOWLEDGEMENTS

This work was sponsored by the National Natural Science Foundation of China under grant nos. 52106098 and 11604179, and the Natural Science Foundation of Shandong Province under grant nos. ZR2021QE021 and ZR2016AQ18. ZQ also acknowledges the Postdoctoral Innovation Project of Shandong Province and the Postdoctoral Applied Research Project of Qingdao. The scientific

calculations in this paper have been done on the HPC Cloud Platform of Shandong University.

## DATA AVAILABILITY

The total rate coefficient for radiative association of  $P^+(3s^23p^2\ ^3P)$  and  $O(2s^22p^4\ ^3P)$  is available in this article and in its online supplementary material.

## REFERENCES

- Agúndez M., Cernicharo J., Guélin M., 2007, *ApJ*, 662, L91  
 Agúndez M., Cernicharo J., Decin L., Encrenaz P., Teyssier D., 2014, *ApJ*, 790, L27  
 Andreatza C., de Almeida A., 2014, *MNRAS*, 437, 2932  
 Andreatza C., de Almeida A., Vichiatti R., Ceccatto D., 2012, *MNRAS*, 427, 833  
 Andreatza C., de Almeida A., Borin A. C., 2016, *MNRAS*, 457, 3096  
 Andreatza C., de Almeida A., Vichiatti R. M., 2018, *MNRAS*, 477, 548  
 Andreatza C. M., de Almeida A. A., Costa G. J., Borin A. C., 2020, *Theor. Chem. Acc.*, 139, 97  
 Antipov S. V., Sjölander T., Nyman G., Gustafsson M., 2009, *J. Chem. Phys.*, 131, 074302  
 Babb J. F., McLaughlin B. M., 2017, *MNRAS*, 468, 2052  
 Babb J. F., Smyth R. T., McLaughlin B., 2019a, *ApJ*, 876, 38  
 Babb J. F., Smyth R., McLaughlin B., 2019b, *ApJ*, 884, 155  
 Bai T., Qin Z., Liu L., 2021, *MNRAS*, 500, 2496  
 Bai T., Qin Z., Liu L., 2022, *MNRAS*, 510, 1649  
 Bains W. et al., 2022, *Phosphorus Sulfur Silicon Relat. Elem.*, 197, 438  
 Baptista L., de Almeida A. A., 2023, *J. Phys. Chem. A*, 127, 1000  
 Barinová Ľ., van Hemert M. C., 2006, *ApJ*, 636, 923  
 Bergner J. B., Öberg K. I., Walker S., Guzmán V. V., Rice T. S., Bergin E. A., 2019, *ApJ*, 884, L36  
 Bernal J., Koelemay L., Ziurys L., 2021, *ApJ*, 906, 55  
 Bregman J., Lester D., Rank D., 1975, *ApJ*, 202, L55  
 Chantzos J., Rivilla V. M., Vasyunin A., Redaelli E., Bizzocchi L., Fontani F., Caselli P., 2020, *A&A*, 633, A54  
 Cherchneff I., Dwek E., 2009, *ApJ*, 703, 642  
 Chyba C. F., Thomas P. J., Brookshaw L., Sagan C., 1990, *Science*, 249, 366  
 Dressler K., 1955, *Helv. Phys. Acta.*, 28, 563  
 Dyke J. M., Morris A., Ridha A., 1982, *J. Chem. Soc. Faraday Trans.*, 78, 2077  
 Fontani F., Rivilla V., Caselli P., Vasyunin A., Palau A., 2016, *ApJ*, 822, L30  
 Fontani F., Rivilla V. M., van der Tak F. F. S., Mininni C., Beltrán M., Caselli P., 2019, *MNRAS*, 489, 4530  
 Forrey R., Babb J., Stancil P., McLaughlin B., 2018, *MNRAS*, 479, 4727  
 Franz J., Gustafsson M., Nyman G., 2011, *MNRAS*, 414, 3547  
 Gerlich D., Horning S., 1992, *Chem. Rev.*, 92, 1509  
 Greaves J. S. et al., 2021a, *Nat. Astron.*, 5, 636  
 Greaves J. S. et al., 2021b, *Nat. Astron.*, 5, 655  
 Gustafsson M., 2020, *J. Chem. Phys.*, 153, 114305  
 Gustafsson M., Forrey R. C., 2019, *J. Chem. Phys.*, 150, 224301  
 Gustafsson M., Monge-Palacios M., Nyman G., 2014, *J. Chem. Phys.*, 140, 184301  
 Haasler D. et al., 2022, *A&A*, 659, A158  
 Halfen D., Clouthier D., Ziurys L. M., 2008, *ApJ*, 677, L101  
 Hansson A., Watson J. K. G., 2005, *J. Mol. Spectrosc.*, 233, 169  
 Herzberg G., 1950, *Molecular Spectra and Molecular Structure. Vol. 1: Spectra of Diatomic Molecules*, 2nd edn. Van Nostrand Reinhold, New York  
 Hou Z., Qin Z., Liu L., 2023, *A&A*, 672, A25  
 Johnson B. R., 1977, *J. Chem. Phys.*, 67, 4086  
 Johnson B. R., 1978, *J. Chem. Phys.*, 69, 4678  
 Jura M., York D., 1978, *ApJ*, 219, 861  
 Kathir R., Nyman G., Gustafsson M., 2017, *MNRAS*, 470, 3068  
 Knowles P. J., Werner H.-J., 1985, *Chem. Phys. Lett.*, 115, 259



- Kramida A., Ralchenko Y., Reader J., Team N. A., 2022, NIST Atomic Spectra Database, Version 5.10 [online]. Available: <https://physics.nist.gov/asd>
- Laidler K. J., 1996, *Int. Union Pure Appl. Chem.*, 68, 149
- Langhoff S. R., Davidson E. R., 1974, *Int. J. Quant. Chem.*, 8, 61
- Lebouteiller V., Ferlet R., Kuassivi M., 2006, in Sonneborn G., Moos H., Andersson B.-G., eds, ASP Conf. Ser. Vol. 348, *Astrophysics in the Far Ultraviolet: Five Years of Discovery with FUSE*. Astron. Soc. Pac., San Francisco, p. 480
- Lefloch B. et al., 2016, *MNRAS*, 462, 3937
- Liljegren S., Jerkstrand A., Barklem P. S., Nyman G., Brady R., Yurchenko S. N., 2022, The molecular chemistry of Type Ibc supernovae, and diagnostic potential with the James Webb Space Telescope, preprint (arXiv:2203.07021)
- McElroy D., Walsh C., Markwick A., Cordiner M., Smith K., Millar T., 2013, *A&A*, 550, A36
- Martin P. A., Fehér M., 2001, *J. Mol. Struct. (Theochem)*, 540, 139
- Meng H., Qin Z., Liu L., 2022, *ApJ*, 935, 148
- Metropoulos A., Papakondylis A., Mavridis A., 2003, *J. Chem. Phys.*, 119, 5981
- Milam S., Halfen D., Tenenbaum E., Apponi A., Woolf N., Ziurys L., 2008, *ApJ*, 684, 618
- Nyman G., Gustafsson M., Antipov S. V., 2015, *Int. Rev. Phys. Chem.*, 34, 385
- Peterson K. A., Woods R. C., 1988, *J. Chem. Phys.*, 89, 4929
- Peterson K. A., Woods R. C., 1990, *J. Chem. Phys.*, 92, 6061
- Petrmichl R. H., Peterson K. A., Woods R. C., 1991, *J. Chem. Phys.*, 94, 3504
- Qin Z., Bai T., Liu L., 2021, *MNRAS*, 507, 2930
- Reiher M., Wolf A., 2004a, *J. Chem. Phys.*, 121, 2037
- Reiher M., Wolf A., 2004b, *J. Chem. Phys.*, 121, 10945
- Rivilla V. M., Fontani F., Beltrán M., Vasyunin A., Caselli P., Martín-Pintado J., Cesaroni R., 2016, *ApJ*, 826, 161
- Rivilla V. M. et al., 2018, *MNRAS*, 475, L30
- Rivilla V. M. et al., 2020, *MNRAS*, 492, 1180
- Rivilla V. M. et al., 2022, *Front. Astron. Space Sci.*, 9, 160
- Salop A., Pollack E., Bederson B., 1961, *Phys. Rev.*, 124, 1431
- Sil M. et al., 2021, *AJ*, 162, 119
- Šimsová-Zámečnicková M., Soldán P., Gustafsson M., 2022, *A&A*, 664, A5
- Spielfiedel A., Handy N. C., 1999, *Phys. Chem. Chem. Phys.*, 1, 2401
- Szabó P., Gustafsson M., 2017, *J. Chem. Phys.*, 147, 094308
- Szabó P., Gustafsson M., 2019, *MNRAS*, 483, 3574
- Szabó P., Góger S., Gustafsson M., 2021, *Front. Astron. Space Sci.*, 8, 704953
- Thorne L., Anicich V., Prasad S., Huntress Jr W., 1984, *ApJ*, 280, 139
- Tomza M., Jachymski K., Gerritsma R., Negretti A., Calarco T., Idziaszek Z., Julienne P. S., 2019, *Rev. Mod. Phys.*, 91, 035001
- Turner B., Bally J., 1987, *ApJ*, 321, L75
- Villanueva G. et al., 2021, *Nat. Astron.*, 5, 631
- Wang K., Wang X., Fan Z., Zhao H.-Y., Miao L., Yin G.-J., Moro R., Ma L., 2021, *Eur. Phys. J. D*, 75, 1
- Watson J. K., 2008, *J. Mol. Spectrosc.*, 252, 5
- Werner H.-J., Knowles P. J., 1985, *J. Chem. Phys.*, 82, 5053
- Werner H. et al., 2015, MOLPRO, version 2015.1, A Package of Ab Initio Programs. Available at <http://www.molpro.net>
- Werner H.-J. et al., 2020, *J. Chem. Phys.*, 152, 144107
- Wetmore R. W., Fox J. L., Dalgarno A., 1984, *Planet. Space Sci.*, 32, 1111
- Wong M. W., Radom L., 1990, *J. Phys. Chem.*, 94, 638
- Zámečnicková M., Soldán P., Gustafsson M., Nyman G., 2019, *MNRAS*, 489, 2954
- Zámečnicková M., Gustafsson M., Nyman G., Soldán P., 2020, *MNRAS*, 492, 3794
- Zhang M., Shi D., 2021, *J. Quant. Spectrosc. Radiat. Transfer*, 264, 107553
- Zhang S., Qin Z., Liu L., 2022, *MNRAS*, 515, 6066
- Zhu Z., Cheng C., Wang S., Shi D., 2014, *Eur. Phys. J. D*, 68, 1
- Ziurys L. M., 1987, *ApJ*, 321, L81

This paper has been typeset from a  $\text{\TeX}/\text{\LaTeX}$  file prepared by the author.